Structures and Properties of Zirconia-Supported Ruthenium Oxide Catalysts for the Selective Oxidation of Methanol to Methyl Formate

Weizhen Li,[†] Haichao Liu,*[,†] and Enrique Iglesia[‡]

Beijing National Laboratory for Molecular Sciences, State Key Laboratory for Structural Chemistry of Stable and Unstable Species, College of Chemistry and Molecular Engineering, Green Chemistry Center, Peking University, Beijing 100871, China, and Department of Chemical Engineering, University of California at Berkeley, Berkeley, California 94720

Received: July 30, 2006; In Final Form: September 15, 2006

The effects of RuO_x structure on the selective oxidation of methanol to methyl formate (MF) at low temperatures were examined on ZrO_2-supported RuO_x catalysts with a range of Ru surface densities (0.2−3.8 Ru/nm^2). Their structure was characterized using complementary methods (X-ray diffraction, Raman and X-ray photoelectron spectra, and reduction dynamics). The structure and reactivity of RuO_x species change markedly with Ru surface density. RuO_x existed preferentially as RuO_4^{2-} species below 0.4 Ru/nm^2, probably as isolated $Zr(RuO_4)_2$ interacting with ZrO_2 surfaces. At higher surface densities, highly dispersed RuO_2 domains coexisted with RuO_4^{2-} and ultimately formed small clusters and became the prevalent form of RuO_x above 1.9 Ru/nm^2. CH_3OH oxidation rates per Ru atom and per exposed Ru atom (turnover rates) decreased with increasing Ru surface density. This behavior reflects a decrease in intrinsic reactivity as RuO_x evolved from RuO_4^{2-} to RuO_2, a conclusion confirmed by transient anaerobic reactions of CH_3OH and by an excellent correlation between reaction rates and the number of RuO_4^{2-} species in RuO_x/ZrO_2 catalysts. The high intrinsic reactivity of RuO_4^{2-} structures reflects their higher reducibility, which favors the reduction process required for the kinetically relevant C−H bond activation step in redox cycles using lattice oxygen atoms involved in CH_3OH oxidation catalysis. These more reactive RuO_4^{2-} species and the more exposed ZrO_2 surfaces on samples with low Ru surface density led to high MF selectivities (e.g. ∼96% at 0.2 Ru/nm^2). These findings provide guidance for the design of more effective catalysts for the oxidation of alkanes, alkenes, and alcohols by the synthesis of denser $Zr(RuO_4)_2$ monolayers on ZrO_2 and other high surface area supports.

Introduction

Methyl formate ($HCOOCH_3$; MF) is an important chemical precursor to other chemicals, such as carboxylic acids, esters, and formamides,[1−4] and in the synthesis of ethylene glycol. MF synthesis currently involves the carbonylation of methanol with CO using strong liquid bases such as sodium methoxide or nonoxidative dehydrogenation of methanol on CuO-based catalysts.[2−5] These processes involve waste byproducts, energy inefficiencies, or thermodynamic constraints. Oxidation processes are catalyzed by dispersed VO_x and MoO_x domains[4−7] with favorable thermodynamics and modest MF selectivities, but improvements in reaction rates and selectivities are required for industrial practice.

The oxidation of methanol to MF on VO_x and MoO_x catalysts involves rate-determining C−H bond activation steps to form HCHO and their subsequent reactions with intermediates derived from CH_3OH or HCHO,[1,8,9] which also form CO_x ($CO + CO_2$) at the conditions required for HCHO formation. RuO_x domains dispersed on ZrO_2, TiO_2, SnO_2, Al_2O_3, or SiO_2 catalyze CH_3OH oxidation to HCHO at unprecedented low temperatures (330−400 K). HCHO then converts to dimethoxymethane (DMM) or MF via methoxymethanol or hemiacetal intermediates (Scheme 1).[10] Supports influence secondary reactions of HCHO and other intermediates and also the redox properties of RuO_x domains. ZrO_2 supports led to the highest MF rates and yields, but also to the highest selectivity to undesired CO_2.[10]

SCHEME 1: Primary and Secondary CH_3OH Reaction Pathways on Supported RuO_x Catalysts

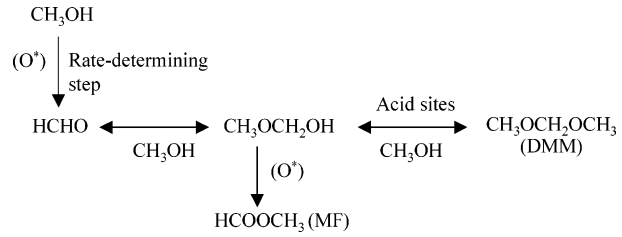

The specific control of structure and atomic connectivity in dispersed oxides remains a critical challenge in the improvement of catalytic performance.[11−17] Here, we probe the relationship between the structure of RuO_x domains supported on ZrO_2 and their redox and catalytic properties during the oxidation of methanol to MF, with the aim to design more effective catalysts for MF synthesis. The structure of RuO_x domains with a range of Ru surface densities (∼0.2−4 Ru/nm^2) was characterized by X-ray diffraction (XRD) and X-ray photoelectron (XPS) and Raman spectroscopies. The reducibility of RuO_x species was probed by temperature-programmed reduction (TPR) in H_2. RuO_4^{2-} structures, containing Ru^{6+} and likely present as $Zr(RuO_4)_2$, were detected and found to be active and selective for MF synthesis.

* Author to whom correspondence should be addressed (e-mail hcliu@pku.edu.cn; telephone/fax 86-10-6275-4031).
[†] Peking University.
[‡] University of California at Berkeley.

10.1021/jp0648689 CCC: $33.50
Published on Web 10/24/2006

Experimental Methods

Synthesis and Characterization of Catalysts. ZrO_2-supported RuO_x catalysts (denoted RuO_x/ZrO_2) were prepared by incipient wetness impregnation of ZrO_2 with an aqueous solution of $Ru(NO)(NO_3)_3$ (Alfa Aesar, 31.3% Ru) at 298 K for 3 h. The Ru concentrations in the impregnating solution were varied to change the Ru content. Impregnated samples were treated in ambient air at 398 K overnight and then at 673 K for 6 h. ZrO_2 was prepared by hydrolysis of aqueous $ZrOCl_2 \cdot 8H_2O$ (Beijing Chemicals, Beijing, China) with excess $NH_3 \cdot H_2O$ (14 N, Beijing Chemicals), followed by washing of the precipitates with deionized water until Cl^- was no longer detected in the filtrate. These precipitates were dried at 393 K overnight and then treated at 673 K in ambient air for 6 h.

BET surface areas were measured by N_2 physisorption at its normal boiling point (at 101 kPa) using an ASAP 2010 analyzer (Micromeritics) after samples were treated at 393 K for 4 h in dynamic vacuum (<2.66 Pa).

XRD patterns were obtained in the 2θ range of 10−80° on a Rigaku D/MAX-2000 diffractometer using Cu Kα radiation ($\lambda = 1.5406$ Å) operated at 30 kV and 100 mA. The average particle sizes (D) were estimated by the Scherrer equation,[18] $D = 0.90\lambda/\beta \cos\theta$, where θ is the diffraction angle and β is the full width at half-maximum (fwhm).

XPS spectra were measured using an Axis Ultra spectrometer (Kratos, Manchester, U.K.) and monochromatic Al Kα (1486.71 eV) radiation at a source power of 225 W (15 mA, 15 kV). The binding energies were referred to a C*1s* peak at 284.8 eV for adventitious carbon. Surface compositions were calculated from peak intensities using the sensitivity factors provided by the spectrometer.

Raman spectra were measured at ambient temperature using a Renishaw 1000 spectrometer equipped with a He−Ne laser at a wavelength of 632.8 nm (model 127-25RP) and a CCD camera. The resolution was 2 cm^{-1}, and the laser power was set to 1.2 mW. Raman shifts for all of the samples were measured in the range of 100−1500 cm^{-1} in ambient air.

Methanol Oxidation Rates and Selectivities. Methanol oxidation rate and selectivity data were measured in a packed-bed quartz microreactor (6 mm i.d.) using catalyst powders (80−100 mesh, 0.2 g), which were diluted with quartz (~2 g) to prevent temperature gradients and hot spots, and treated in 10% O_2/N_2 (Beijing Huayuan, 99.999%) flow (30 cm^3 min^{-1}) at 673 K for 1 h before catalytic measurements. Reactants consisted of 3.5 kPa of CH_3OH (Beijing Chemicals, 99.99%) and 10 kPa of O_2 (Beijing Huayuan, 99.999%) with 86.5 kPa of balance N_2 (Beijing Huayuan, 99.999%). All transfer lines between the reactor and gas chromatograph were kept above 393 K to avoid condensation of the products. Reactants and products were analyzed by on-line gas chromatography (Shimadzu 2010 GC) using two packed columns (Carbosieve B, O_2, N_2, and CO; Porapak N, other components) connected to thermal conductivity detectors (TCD). Steady-state kinetic data were collected after 2 h on-stream. Selectivities are reported on a carbon basis and rates as molar CH_3OH conversion rates per mole of Ru per hour. Blank experiments were conducted using empty reactors, quartz powders, and pure ZrO_2 support without detectable CH_3OH conversions at all conditions in this study.

Dynamics of Reduction of Dispersed RuO_x Domains in H_2. H_2 temperature-programmed reduction (TPR) data were measured using a flow unit (TP5000, Tianjin Xianquan). Samples were placed within a quartz cell, and the temperature was increased linearly from 293 to 773 K at 10 K min^{-1} in flowing 5% H_2/N_2 (50 cm^3 min^{-1}; Beijing Huayuan, certified mixture). The amount of sample was varied so as to keep similar amounts of Ru (ca. 4 mg) within the cell for samples with various Ru contents. The H_2 concentration in the effluent was measured by on-line mass spectrometry (Hiden HPR 20). The spectrometer response was calibrated by reducing CuO powders (Beijing Chemicals, >99.0%) in H_2 (5% H_2/N_2).

TABLE 1: BET Surface Areas, Nominal Ru Suface Densities, Average ZrO_2 Crystallite Sizes, and XPS $Ru3d_{5/2}$ Binding Energies for ZrO_2-Supported RuO_x Catalysts

Ru loading (wt %)	surface area (m^2/g)	Ru surface density (Ru/nm^2)	average size[a] (nm)	binding energy (eV) species I	binding energy (eV) species II
0	116.0	0	7.9		
0.4	121.0	0.2	7.2	282.7	
0.9	121.4	0.4	6.8	282.7	280.9
1.9	120.2	0.9	7.1	282.7	280.8
3.5	109.3	1.9	6.8	282.8	280.9
5.5	105.3	3.1	6.8	282.8	280.9
6.7	106.6	3.8	7.3	282.7	281.0

[a] Calculated from X-ray diffraction patterns for these samples by the Sherrer equation.

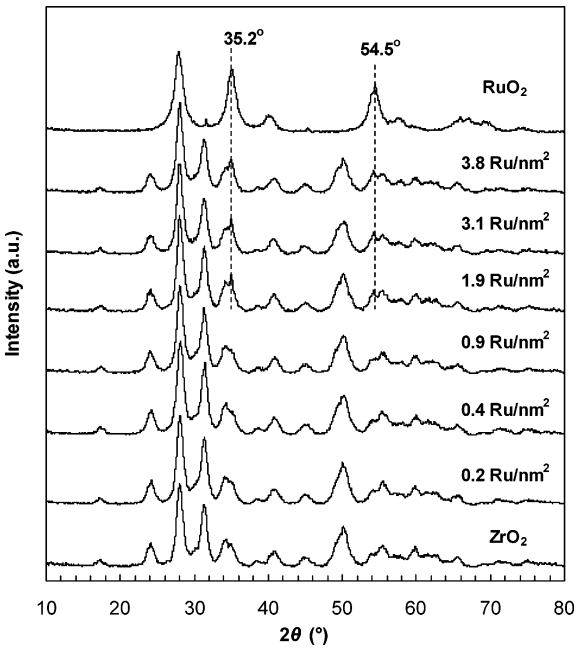

Figure 1. X-ray diffraction patterns for ZrO_2-supported RuO_x catalysts with Ru surface densities of 0.2−3.8 Ru/nm^2 and for pure ZrO_2 and RuO_2.

Results and Discussion

Catalyst Characterization. BET surface areas and nominal RuO_x surface densities are reported in Table 1 for all RuO_x/ZrO_2 samples. The nominal RuO_x surface densities (Ru/nm^2) were estimated from the Ru content and BET surface area. The surface areas, specifically for the samples with Ru surface density above 1.9 Ru/nm^2, decreased slightly with increasing Ru content and surface density, as a result of the deposition of dispersed RuO_x on top of ZrO_2 surfaces.

Figure 1 shows diffraction patterns for RuO_x/ZrO_2, ZrO_2, and RuO_2 [from decomposition of $Ru(NO)(NO_3)_3$ at 673 K]. ZrO_2 showed only monoclinic structures without detectable tetragonal phase ($2\theta = 30.2°$).[19] Pure RuO_2 gave intense lines at $2\theta =$ 28.1°, 35.2°, 40.5°, and 54.5°; the lines at 35.2° and 54.5° do not overlap those for monoclinic ZrO_2 and can be used to detect crystalline RuO_2. RuO_x/ZrO_2 samples with low RuO_x

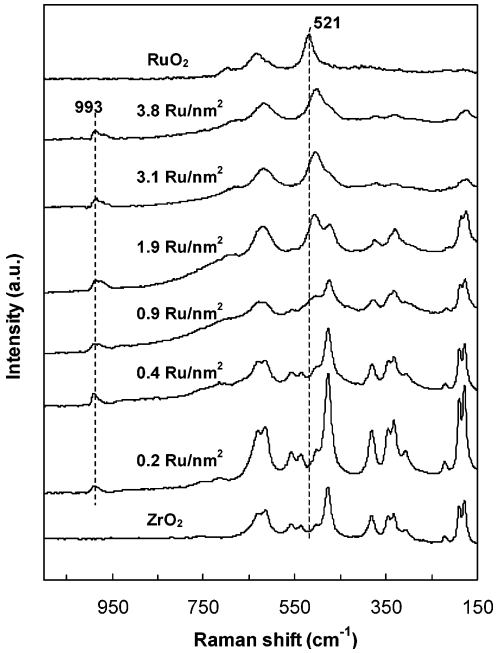

Figure 2. Raman spectra for ZrO_2-supported RuO_x catalysts with Ru surface densities of 0.2−3.8 Ru/nm^2 and for pure ZrO_2 and RuO_2.

concentrations (<1.9 Ru/nm^2) showed only monoclinic ZrO_2 and no crystalline RuO_x, suggesting that RuO_x species were well dispersed on ZrO_2. RuO_2 diffraction lines appeared at 1.9 Ru/nm^2 and became more intense as RuO_2 crystallites formed with increasing Ru surface density. The line breadth for the diffraction line at $2\theta = 28.1°$ was used to estimate ZrO_2 crystallite sizes, which ranged from 6.8 to 7.9 nm (Table 1), irrespective of RuO_x surface density.

Raman spectra (Figure 2) confirmed that only monoclinic ZrO_2 was present in the ZrO_2 support. Crystalline RuO_2 showed three Raman bands at 521, 640, and 704 cm^{-1}, corresponding to E_g, A_{1g}, and B_{2g} modes;[20] the band at 521 cm^{-1} does not overlap with the ZrO_2 bands, and it can be used to detect crystalline RuO_2 in RuO_x/ZrO_2. It was not detected for Ru surface densities of 0.2 and 0.4 Ru/nm^2, but emerged as a weak shoulder at 0.9 Ru/nm^2 and became stronger above 1.9 Ru/nm^2, suggesting that crystalline RuO_2 forms at surface densities >0.9 Ru/nm^2. The observed red shift of this band relative to bulk crystalline RuO_2 appears to reflect the small size of supported RuO_2 crystallites.[20] A band was observed at ∼993 cm^{-1} in all RuO_x/ZrO_2 samples. Taken together with the XPS spectra and stoichiometric H_2 reduction data, this new band can be tentatively assigned to terminal Ru═O stretching vibrations for RuO_4^{2-} species (Ru^{6+}) probably present in $Zr(RuO_4)_2$ structures formed via reactions of ZrO_2 with RuO_x during treatment in air at 673 K.

The presence of RuO_2 and RuO_4^{2-} species in RuO_x/ZrO_2 was confirmed by XPS. At low Ru surface densities (e.g., 0.2 Ru/nm^2), only a $Ru3d_{5/2}$ signal with a binding energy of 282.7 eV corresponding to Ru^{6+} [21] was observed (Table 1). The structure of the Ru^{6+} species remains unclear, but it is unlikely to be RuO_3 because of its thermodynamic instability and high volatility. This supports the presence of only RuO_4^{2-} species in this sample. As Ru surface density increased to 0.4 Ru/nm^2, RuO_2 structures formed, as shown by a feature with a $Ru3d_{5/2}$ binding energy of 281.0 eV.[21] The surface $Ru^{6+}/(Ru^{6+} + Ru^{4+})$ atomic ratio was estimated to be 0.90 for this sample; this value decreased monotonically to 0.39 as the surface density increased to 3.8 Ru/nm^2 (Figure 3). Thus, the fraction of the Ru present

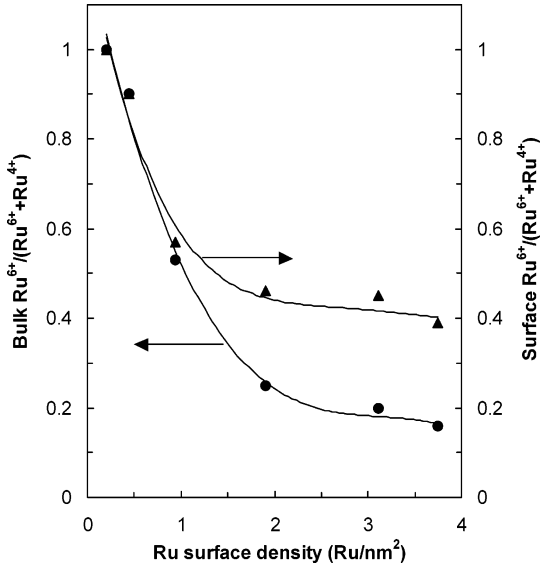

Figure 3. Surface (measured by XPS) and bulk (measured by H_2 TPR) RuO_x fractions for ZrO_2-supported RuO_x catalysts.

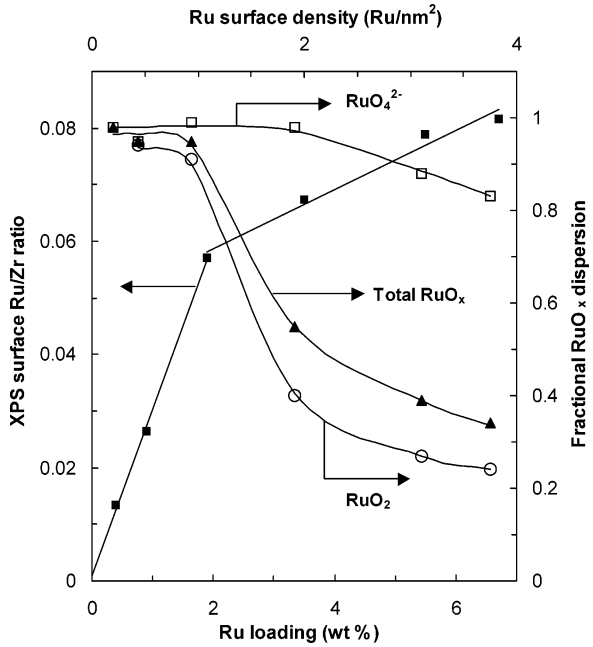

Figure 4. Surface Ru/Zr ratios (measured by XPS) and fractional dispersions of total RuO_x species and of respective RuO_4^{2-} and RuO_2 species (estimated by surface Ru/Zr ratios from XPS) as a function of Ru content and surface density.

as Ru^{4+} increases with increasing Ru surface density at ZrO_2 surfaces.

Figure 4 shows surface Ru/Zr atomic ratios (including Ru^{4+} and Ru^{6+}) for these samples as a function of Ru surface density. These Ru/Zr ratios were initially proportional to the Ru surface density and then increased more slowly for surface densities above 1.9 Ru/nm^2. The initial linear increase indicates that RuO_x species are highly dispersed on ZrO_2 at surface densities below 1.9 Ru/nm^2 and then aggregate to form RuO_2 crystallites at higher surface coverages, as also observed by XRD and Raman. Such behavior is consistent with Stranski−Krastanov (SK) growth mechanisms,[22] in which RuO_4^{2-} and RuO_2 are dispersed up to 0.9 Ru/nm^2 and then three-dimensional clusters form. The "saturation" coverage at which crystallites form is much smaller than the theoretical monolayer coverage of ∼4−5 Ru/nm^2 [for the RuO_2 (110) plane].[10] RuO_x dispersions were estimated from

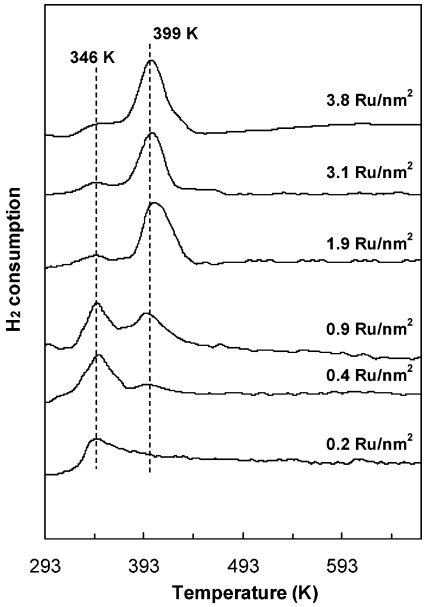

Figure 5. H_2 temperature-programmed reduction profiles for ZrO_2-supported RuO_x catalysts with Ru surface densities of 0.2−3.8 Ru/nm^2 treated at 673 K in air.

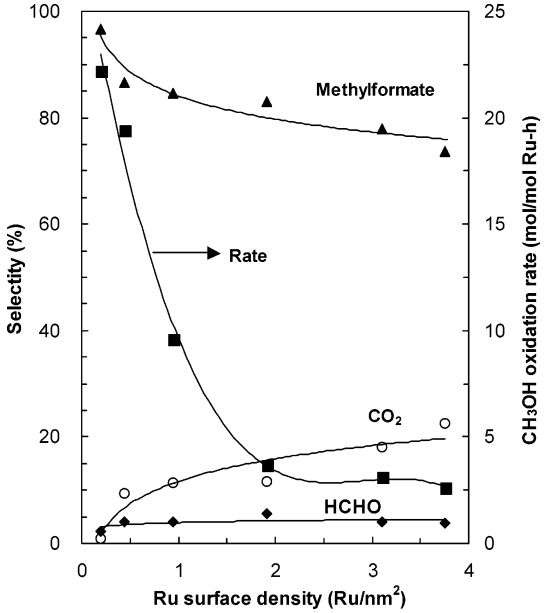

Figure 6. CH_3OH oxidation rates normalized per Ru atom and selectivities as a function of Ru surface density at 373 K on RuO_x/ZrO_2 catalysts at conversions of ∼15% (0.2−3.8 Ru/nm^2, 3.5 kPa of CH_3OH, 10 kPa of O_2, balance N_2).

surface Ru/Zr ratios measured by XPS using a method previously reported.[23,24] Figure 4 shows that fractional dispersions of toal RuO_x species were essentially constant at near unity (0.95−0.98) up to 0.9 Ru/nm^2 and then decreased monotonically to a value of 0.34 as surface densities reached 3.8 Ru/nm^2. This is consistent with the growth of RuO_2 crystallites, as shown from the respective dispersions of the coexisting RuO_4^{2-} and RuO_2 species. RuO_2 dispersions deceased sharply above 0.9 Ru/nm^2, but RuO_4^{2-} species remained highly dispersed (0.85) even at 3.8 Ru/nm^2, apparently because of their strong interactions with ZrO_2 surfaces.

The bulk composition and oxidation state of RuO_x species in RuO_x/ZrO_2 were examined by temperature-programmed reduction (TPR) using H_2 as the reductant. Only one reduction peak (at ∼346 K) was present for the sample with 0.2 Ru/nm^2 (Figure 5), and the reduction stoichiometry was 2.95 H_2/Ru, similar to the value expected for stoichiometric reduction of RuO_4^{2-} to Ru^0:

$$Zr(RuO_4)_2 + 3\,H_2 \rightarrow ZrO_2 + Ru + 3\,H_2O$$

Another reduction peak appeared at a surface density of 0.4 Ru/nm^2 as a shoulder (at ∼400 K). Its reduction stoichiometry is consistent with the reduction of RuO_2 to Ru metal. This RuO_2 reduction feature became more intense relative to the RuO_4^{2-} reduction peak with increasing Ru surface density (Figure 5). This can also be seen clearly from the bulk $Ru^{6+}/(Ru^{6+} + Ru^{4+})$ atomic ratios presented in Figure 3, showing that RuO_2 species become prevalent on ZrO_2 as Ru surface density increases.

Taken together, these characterization results indicate that RuO_x species evolve from dispersed RuO_4^{2-} species, probably in $Zr(RuO_4)_2$ structures, at Ru surface densities below 0.4 Ru/nm^2 to dispersed and three-dimensional RuO_2 domains at Ru surface densities >1.9 Ru/nm^2.

Methanol Oxidation Rates and Selectivities on RuO_x/ZrO_2 Catalysts. Figure 6 shows methanol oxidation rates (per Ru atom) and selectivities at 373 K as a function of Ru surface density on RuO_x/ZrO_2 catalysts. The rates and selectivities were compared at similar CH_3OH conversions (∼15%) because the extent of CH_3OH conversion influences the relative contributions of primary and secondary reactions.[10] The rates and selectivities remained essentially unchanged with time (for 48 h) on all samples. CH_3OH oxidation rates (per Ru atom) decreased sharply as Ru surface density increased from 0.2 to 1.9 Ru/nm^2 and then more gradually at higher Ru surface densities. MF selectivities decreased monotonically from 96.6 to 72.6% with increasing Ru surface density (from 0.2 to 3.8 Ru/nm^2) while CO_2 selectivities concurrently increased (from 0.8 to 23.6%). HCHO selectivities were low, which initially increased slightly with increasing Ru surface density, and then reached a constant value of 4.1% above 0.4 Ru/nm^2 (Figure 6). By referring to the structural evolution of the RuO_x domains with the Ru surface density and dispersion, these results indicate that the dispersed RuO_4^{2-} species seem to be more selective for the MF synthesis relative to the RuO_2 species. The higher MF selectivities on samples with low Ru surface density may also be due to their higher exposed ZrO_2 surface areas involved in the conversion of HCHO intermediates to MF.[10]

At Ru surface densities below 1.9 Ru/nm^2, especially for 0.2−0.9 Ru/nm^2, nearly all of the Ru atoms in RuO_x domains are accessible to reactants. For these samples, rates per Ru atom correspond to turnover rates and reflect the intrinsic reactivity of exposed RuO_x species. Therefore, the decrease in the rates in the Ru surface density range from 0.2 to 0.9 Ru/nm^2 reflects a decrease in reactivity as a result of the structural change from RuO_4^{2-} species to RuO_2 species with lower reactivity. Above 1.9 Ru/nm^2, dispersed and crystalline RuO_2 domains became the prevalent structures. The observed decrease in methanol oxidation rates (per Ru atom) with increasing Ru surface density may reflect either the lower intrinsic reactivity of RuO_2 domains relative to RuO_4^{2-} or merely their lower dispersion. Turnover rates [i.e., rates normalized by exposed Ru atoms (including both Ru^{4+} and Ru^{6+} species) using Ru dispersion data in Figure 4] still decreased with increasing Ru surface densities (Figure 7), suggesting that the intrinsic reactivity for RuO_4^{2-} is higher than that for RuO_2 domains. In this case, CH_3OH oxidation rates (per Ru atom) should increase in parallel with the RuO_4^{2-} fractions in these samples, as indeed shown by the data in Figure 8.

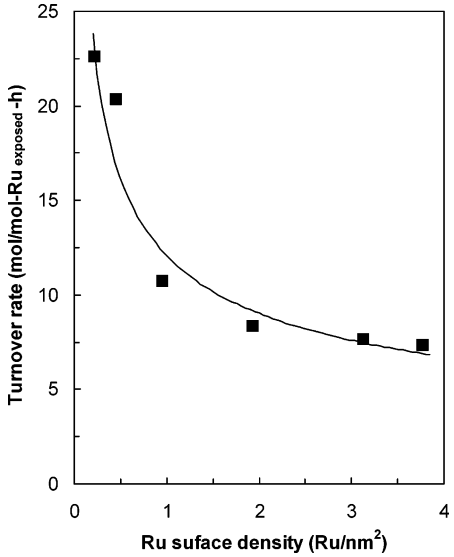

Figure 7. CH_3OH oxidation turnover rates (per exposed Ru atom) as a function of Ru surface density at 373 K on RuO_x/ZrO_2 catalysts at conversions of ~15% (0.2−3.8 Ru/nm^2, 3.5 kPa of CH_3OH, 10 kPa of O_2, balance N_2).

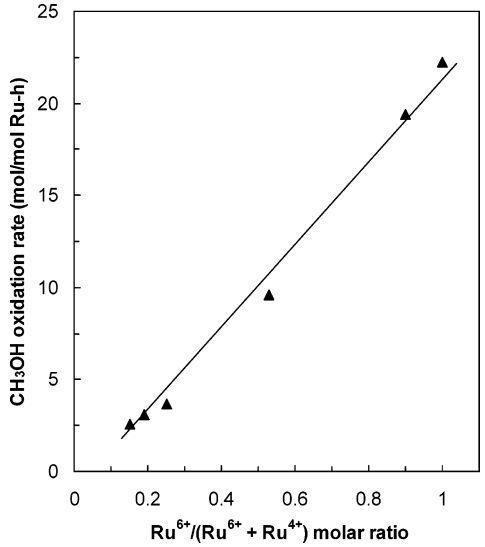

Figure 8. Dependence of CH_3OH oxidation rates normalized per Ru atom at 373 K on the fractions of RuO_4^{2-} species [represented as $Ru^{6+}/(Ru^{6+} + Ru^{4+})$ molar ratios] for RuO_x/ZrO_2 catalysts (0.2−3.8 Ru/nm^2, 3.5 kPa of CH_3OH, 10 kPa of O_2, balance N_2, ~15% CH_3OH conversions).

The higher intrinsic reactivity of RuO_4^{2-} relative to RuO_2 is consistent with its more reducible nature. The peak temperature for RuO_4^{2-} reduction was about 50 K below that for RuO_2 reduction (Figure 5). The more reducible nature of RuO_4^{2-} appears to reflect its higher Ru oxidation state and the atomic connectivity between Ru^{6+} and the less electronegative nature of Zr^{4+} cations in $Zr(RuO_4)_2$ relative to Ru cations in oligomeric RuO_x structures, which may favor electron transfer and activation of Ru−O bonds during reduction in H_2 and CH_3OH oxidation catalysis compared with RuO_2 structures. Clearly, Ru^{6+} species are more reducible than Ru^{4+}, but cannot be stabilized against autoreduction without the formation of mixed structures with ZrO_2. A correlation between reducibility and methanol oxidation rates is consistent with a Mars−van Krevelen cycle. It has been previously demonstrated for CH_3OH oxidation using kinetic and isotopic methods, which showed that HCHO and MF form on RuO_x domains via redox cycles

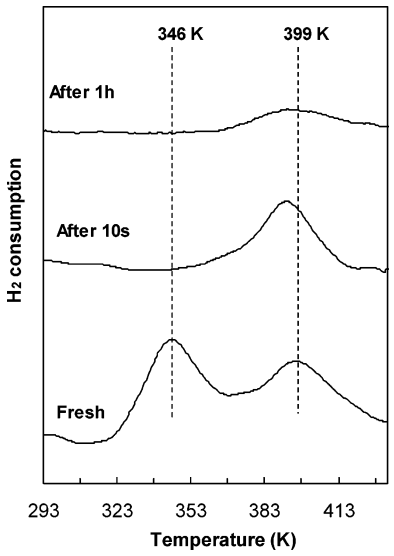

Figure 9. H_2 temperature-programmed reduction profiles for RuO_x/ZrO_2 catalyst with a Ru surface density of 0.9 Ru/nm^2 before and after reactions with a CH_3OH/N_2 (3.5 kPa of CH_3OH/96.5 kPa of N_2) stream for 10 s and 1 h, respectively, at 373 K under anaerobic conditions.

involving lattice oxygen atoms and kinetically relevant C−H bond activation steps.[10] More facile reduction of the RuO_x domains leads to faster CH_3OH oxidation turnovers, because transition states required for C−H bond activation steps involve electron transfer and the local reduction of cationic centers in reducible metal oxides. Similar reactivity−reducibility correlations were observed for selective oxidation reactions of alcohols,[10,23,24] dimethyl ether,[15−17] and light alkanes[25,26] on MoO_x- and VO_x-based materials, which also catalyze oxidation reactions via Mars−van Krevelen redox cycles.

The higher intrinsic reactivity of RuO_4^{2-} structures was also evident from transient anaerobic CH_3OH reactions on dispersed RuO_4^{2-} and RuO_2 structures that coexist in nearly equimolar amounts in the sample with 0.9 Ru/nm^2. These transient experiments were conducted by controlled exposure of samples to CH_3OH to attain a given extent of reduction via reactions between RuO_x domains and CH_3OH under anaerobic conditions. Samples were then reduced in H_2 by increasing the temperature from 298 to 673 K after removal of CH_3OH from the bed with a pure N_2 purge. Figure 9 shows that exposure to a CH_3OH/N_2 (3.5 kPa of CH_3OH/96.5 kPa of N_2) stream for 10 s led to the complete disappearance of the lower temperature RuO_4^{2-} reduction peak, present in the fresh sample, during subsequent reduction, whereas the peak corresponding to RuO_2 reduction remained essentially unchanged. These data show that RuO_4^{2-} species react with CH_3OH preferentially over RuO_2 species. After prolonged contact with the CH_3OH stream, the RuO_2 reduction peak also decreased in intensity (Figure 9), indicating that the RuO_2 species can also participate in the CH_3OH reactions, albeit with lower reactivity. Steady-state catalytic reactions of CH_3OH/O_2 mixtures led to a H_2 reduction profile (not shown in Figure 9) similar to that for the fresh sample, indicating that the reoxidation is fast and kinetically irrelevant during methanol oxidation catalysis and that Ru atoms exist predominately in their higher oxidation state during catalytic turnovers. This is consistent with the involvement of the redox cycles using lattice oxygen atoms in the CH_3OH conversion to MF on RuO_x domains, as discussed above, and with the slow nature and kinetic relevance of the reduction part of the cycle—the activation of C−H bonds in chemisorbed methoxide species. These observed effects of RuO_x structure on reducibility and

catalytic properties may provide a fundamental basis for the design and synthesis of new catalysts for the CH_3OH conversion to MF and other products and also for light alkane selective oxidations, for example, via the synthesis of more complete Zr-$(RuO_4)_2$ monolayers on ZrO_2 or on other support structures with higher surface areas.

Conclusions

ZrO_2-supported RuO_x domains catalyze the oxidation of methanol to methyl formate at low temperatures (e.g., 373 K). CH_3OH oxidation rates and selectivities strongly depend on RuO_x structure, which varied with Ru surface density (0.2−3.8 Ru/nm^2). RuO_x was preferentially dispersed as isolated RuO_4^{2-} species below 0.4 Ru/nm^2, probably as $Zr(RuO_4)_2$. At higher Ru surface densities, highly dispersed RuO_2 domains formed, and then three-dimensional RuO_2 clusters became prevalent above 1.9 Ru/nm^2. Such structural evolution of RuO_x structures from RuO_4^{2-} to RuO_2 with increasing Ru surface density led to a linear decrease in methanol oxidation rates per Ru atom and per exposed Ru atom (turnover rates) as the RuO_4^{2-} fraction decreased, indicating that RuO_4^{2-} species are more reactive than RuO_2 domains in the activation of C−H bonds in methoxide intermediates, previously shown to control methanol oxidation rates on RuO_x. These conclusions are consistent with transient anaerobic CH_3OH reactions and H_2 temperature-programmed reduction data, which show that RuO_4^{2-} is more reducible than RuO_2. The more reactive nature of RuO_4^{2-} species and the higher exposed ZrO_2 surface area on samples with low Ru surface density led to very high methyl formate selectivities (∼96% at 0.2 Ru/nm^2). Taken together, these results show that RuO_4^{2-} structures exhibit unprecedented reaction rates and selectivities for the synthesis of methyl formate from methanol−O_2 co-reactants.

Acknowledgment. This work was supported by the National Natural Science Foundation of China (Grants 20443010 and 20573004). This work was also supported in part by the Key Laboratory of Material-oriented Chemical Engineering of Jiangsu Province and by the Program for New Century Excellent Talents in University (NECT-05-0010) and the Project Sponsored by the Scientific Research Foundation for the Returned Overseas Chinese Scholars, State Education Ministry.

References and Notes

(1) Tatibouet, J. M. *Appl. Catal., A* **1997**, *148*, 213.
(2) Lee, J. S.; Kim, J. C.; Kim, Y. G. *Appl. Catal.* **1990**, *57*, 1.
(3) Gerard, E.; Gotz, H.; Pellegrini, S.; Castanet, Y.; Mortreux, A. *Appl. Catal., A* **1998**, *170*, 297.
(4) Tronconi, E.; Elmi, A. S.; Ferlazzo, N.; Forzatti, P.; Busca, G.; Tittarelli, P. *Ind. Eng. Chem. Res.* **1987**, *26*, 1269.
(5) Ai, M. *J. Catal.* **1982**, *77*, 279.
(6) Valente, N. G.; Arrua, L. A.; Cadus, L. E. *Appl. Catal., A* **2001**, *205*, 201.
(7) Louis, C.; Tatibout, J. M.; Che, M. *J. Catal.* **1988**, *109*, 354.
(8) Busca, G. *Catal. Today* **1996**, *27*, 457.
(9) Liu, Y. C.; Griffin, G. L.; Chan, S. S.; Wachs, I. E. *J. Catal.* **1985**, *94*, 108.
(10) Liu, H.; Iglesia, E. *J. Phys. Chem. B* **2005**, *109*, 2155.
(11) Iwasawa, Y. *Acc. Chem. Res.* **1997**, *30*, 103.
(12) Tada, M.; Iwasawa, Y. *J. Mol. Catal. A: Chem.* **2003**, *204−205*, 27.
(13) Bell, A. T. *Science* **2003**, *299*, 1688.
(14) Mestl, G.; Srinivasan, T. K. K. *Catal. Rev.−Sci. Eng.* **1998**, *40*, 451.
(15) Liu, H.; Cheung, P.; Iglesia, E. *J. Catal.* **2003**, *217*, 222.
(16) Liu, H.; Cheung, P.; Iglesia, E. *J. Phys. Chem. B* **2003**, *107*, 4118.
(17) Liu, H.; Cheung, P.; Iglesia, E. *Phys. Chem. Chem. Phys.* **2003**, *5*, 3795.
(18) Guinier, A. *Theorie et Technique de la Radiocristallographie*, 3rd ed.; Dunod: Paris, 1964; p 482.
(19) Xie, S.; Chen, K.; Bell, A. T.; Iglesia, E. *J. Phys. Chem. B* **2000**, *104*, 10059.
(20) Mar, S. Y.; Chen, C. S.; Huang, Y. S.; Tiong, K. K. *Appl. Surf. Sci.* **1995**, *90*, 497.
(21) Chan, H. Y. H.; Takoudis, C. G.; Weavery, M. J. *J. Catal.* **1997**, *172*, 336.
(22) Shido, T.; Okita, G.; Asakura, K.; Iwasawa, Y. *J. Phys. Chem. B* **2000**, *104*, 12263.
(23) Deo, G.; Wachs, I. E. *J. Catal.* **1994**, *146*, 323.
(24) Zhang, W.; Desikan, A.; Oyama, S. T. *J. Phys. Chem.* **1995**, *99*, 14468.
(25) Abello, M. C.; Gomez, M. F.; Cadus, L. E. *Catal. Lett.* **1998**, *83*, 185.
(26) Chen, K.; Xie, S.; Bell, A. T.; Iglesia, E. *J. Catal.* **2001**, *198*, 232.